

P3.2 SENSITIVITY OF WIND AND TEMPERATURE RETRIEVALS FROM 4DVAR TO PRESCRIBED EDDY VISCOSITY PROFILES

Rob K. Newsom*, *CIRA, Colorado State University, Fort Collins, CO, USA*
 Robert M. Banta, *Environmental Technology Laboratory/NOAA, Boulder, CO, USA*

1. INTRODUCTION

A Doppler lidar measures the component of air velocity parallel to the beam (radial velocity) as a function of distance along the beam. Spatially and temporally resolved measurements of radial velocity can be performed by repeatedly scanning the beam through a volume of the atmospheric boundary layer.

A four-dimensional variational data assimilation (4DVAR) algorithm, implementing the adjoint of a large eddy simulation (LES) has been developed for the purpose of retrieving three-dimensional, time varying wind and temperature fields from Doppler lidar radial velocity data. The method consists of finding the optimal initialization of a set of prognostic equations (forward model), which minimizes a cost function. The cost function is a measure of the error between the observed radial velocity field and the radial velocity component of the forward model output. The initial conditions of the forward model are treated as control parameters, which are adjusted to minimize the cost function. Efficient minimization of the cost function is achieved using the so-called adjoint method.

The method outlined above was initially demonstrated by Sun et. al. (1991) and applied to radar data by Sun and Crook (1994). Using simulated measurements Lin et al. (2001) evaluated a modified version of the algorithm for retrieval of small-scale velocity and temperature structures with resolutions characteristic of LES.

In the present study, a variable eddy viscosity has been incorporated into the Reynolds stress. As a simplifying assumption the eddy viscosity is treated as a prescribed variable. The technique is described and then applied to Doppler lidar volume scan data collected under convective conditions during the CASES-99 field experiment in south-central Kansas. This paper presents initial results from a study examining the sensitivity of the retrieved fields to changes in prescribed eddy viscosity profiles.

2. FORWARD MODEL

The forward model simulates dry, shallow incompressible flow under the Boussinesq approximation. The forward model equations are:

$$\frac{\partial u_i}{\partial t} = -\frac{\partial p}{\partial x_i} + H_i, \quad (1)$$

$$H_i = \frac{g\theta'}{\Theta_{ref}} \delta_{i3} + \frac{\partial}{\partial x_j} (2\nu S_{ij} - u_i u_j), \quad (2)$$

$$S_{ij} = \frac{1}{2} \left(\frac{\partial u_i}{\partial x_j} + \frac{\partial u_j}{\partial x_i} \right), \quad (3)$$

$$\frac{\partial \theta'}{\partial t} = \frac{\partial}{\partial x_j} \left(\kappa \frac{\partial \theta}{\partial x_j} - u_j \theta' \right) - w \frac{\partial \theta_o}{\partial z}, \quad (4)$$

$$\nabla^2 p = \frac{\partial H_i}{\partial x_i} + \frac{1}{\Delta t} \frac{\partial u_i}{\partial x_i}. \quad (5)$$

The density normalized perturbation pressure is p , g is the acceleration of gravity, Θ_{ref} is a reference potential temperature. The potential temperature is expressed as $\theta = \theta_o(z) + \theta'(t, \mathbf{r})$, where $\theta_o(z)$ is a prescribed base state and θ' is the departure from the base state. The base state potential temperature $\theta_o(z)$ is obtained from radiosonde measurements. In (5) the Harlow Welch (1965) scheme is used to suppress divergence and Δt is the integration time step size. Equations (1) through (5) are integrated using a second order Adams Bashforth scheme on a staggered grid with periodic lateral boundary conditions. On the top and bottom of the domain $w=0$, $\theta'=0$ and the horizontal velocity components u and v are prescribed and constant. Additionally, the eddy diffusion ν and diffusivity κ coefficients are treated as prescribed variables.

3. COST FUNCTION

The basic problem is to find the initial conditions, $\mathbf{u}(t=0, \mathbf{r})$ and $\theta(t=0, \mathbf{r})$, of equations (1) and (4) that minimize the total squared error between the forward model's prediction of radial velocity and the lidar measurements over the volume and time duration of the measurements. This error is given by the cost function

$$L = \int k_u (u_i \hat{r}_i - u_r^{obs})^2 d^3 r dt + \text{Penalty terms}, \quad (6)$$

where $u_r^{obs}(t, \mathbf{r})$ is the radial velocity measured by the lidar, \hat{r} is a unit vector from the lidar (at the origin) to a point in the model domain, and k_u is a binary weighting parameter that is 1 if a measurement $u_r^{obs}(t, \mathbf{r})$ is available at (t, \mathbf{r}) or zero otherwise. The penalty terms include a constraint of zero divergence at the initial time and spatial smoothness constraints on \mathbf{u} and θ' over the entire assimilation period (Sun et. al 1991; Sun and Crook 1994; Lin et al. 2001). The integration in (6) is carried out over the volume of the model domain and over the assimilation time, T .

4. ADJOINT EQUATIONS

The continuous adjoint equations corresponding to the forward model (1) through (5) are derived in the manner described in Sun et. al. (1991). Taking the first variation of (6) with respect to \mathbf{u} , θ and p , and requiring that $\partial L / \partial \mathbf{u}$, $\partial L / \partial \theta$ and $\partial L / \partial p$ vanish one obtains

* Corresponding author address: Dr. Rob K. Newsom, NOAA/ETL R/ET2, 325 Broadway, Boulder, CO, USA 80305-3328; e-mail: rob.k.newsom@noaa.gov.

the Euler-Lagrange or so-called adjoint equations of the forward model:

$$\begin{aligned} \frac{\partial \lambda_i}{\partial t} = & - \left(u_j + \frac{\partial v}{\partial x_j} \right) \left(\frac{\partial \lambda_i}{\partial x_j} + \frac{\partial \lambda_j}{\partial x_i} - 2 \frac{\partial^2 \lambda_p}{\partial x_i \partial x_j} \right) \\ & - \theta' \frac{\partial \lambda_\theta}{\partial x_i} + \lambda_\theta \frac{\partial \theta_o}{\partial x_i} + \frac{1}{\Delta t} \frac{\partial \lambda_p}{\partial x_i} \\ & - v \left(\nabla^2 \lambda_i - \frac{\partial^2 \lambda_j}{\partial x_i \partial x_j} \right) + 2k_u (u_j \hat{r}_j - u_r^{obs}) \hat{r}_i \end{aligned} \quad (7)$$

$$\begin{aligned} \frac{\partial \lambda_\theta}{\partial t} = & - \left(u_j + \frac{\partial v}{\partial x_j} \right) \frac{\partial \lambda_\theta}{\partial x_j} \\ & - \frac{g}{\Theta_{ref}} \left(\lambda_3 - \frac{\partial \lambda_p}{\partial z} \right) - \kappa \nabla^2 \lambda_\theta \end{aligned} \quad (8)$$

$$\nabla^2 \lambda_p = \frac{\partial \lambda_i}{\partial x_i} \quad (9)$$

$$\frac{\partial L}{\partial u_i(0, \mathbf{r})} = -\lambda_i(0, \mathbf{r}) \quad (10)$$

$$\frac{\partial L}{\partial \theta(0, \mathbf{r})} = -\lambda_\theta(0, \mathbf{r}) \quad (11)$$

The Lagrange multipliers or adjoint variables corresponding to strong constraints given by equations (1), (4) and (5) are λ_i , λ_θ , and λ_p , respectively. In deriving equations (7) through (11), the boundary conditions of the adjoint variables have been chosen to eliminate surface terms. Equations (7) through (11) do not include contributions from the divergence or spatial smoothness constraints. Furthermore, the coefficients of eddy diffusion v and diffusivity κ have been treated as prescribed variables.

Equations (10) and (11) give the gradient of the cost function with respect to the initial state of the forward model in terms of solutions of the adjoint equations (7) through (9). With this information a conjugate gradient method can be used to iteratively search for the minimum of L given some arbitrary starting values of $\mathbf{u}(0, \mathbf{r})$ and $\theta(0, \mathbf{r})$. This is accomplished by first integrating the forward model from $t=0$ to $t=T$, then integrating the adjoint equations from $t=T$ to $t=0$. The initial conditions are then incremented in the direction of steepest descent of L using (10) and (11). This process is repeated until L is minimized. Further details are given by Sun et. al (1991) and Sun and Crook (1994).

5. APPLICATION

The 4DVAR retrieval algorithm outlined above was successfully tested using simulated radial velocity data generated from the forward model given by equations (1) through (5). For the current study, we focus on its application to real data. Computations are carried out on 20x20x20 grid within a domain measuring 3km x 3km x 1km in x , y and z , respectively.

5.1 Data Preprocessing

Data used in this study were obtained under convective conditions during the afternoon of 25 October 1999 at the main CASES-99 site, near Leon, Kansas. A ground-based, scanning coherent Doppler lidar provided radial velocity data from repeated volume scans of the boundary layer. Volume data were acquired using a raster scan technique in which the laser beam scanned a 60° sector centered on an azimuth of 270° in a sequence of elevation angles ranging from 0° to 20° . Figure 1 shows horizontal and vertical cross sections of radial velocity $u_r^{obs}(t, \mathbf{r})$ at the start and end of the assimilation period. The lidar is located at the origin of the coordinate system. We note that the coordinates have been rotated so that the data are contained entirely within the positive octant of the model coordinates.

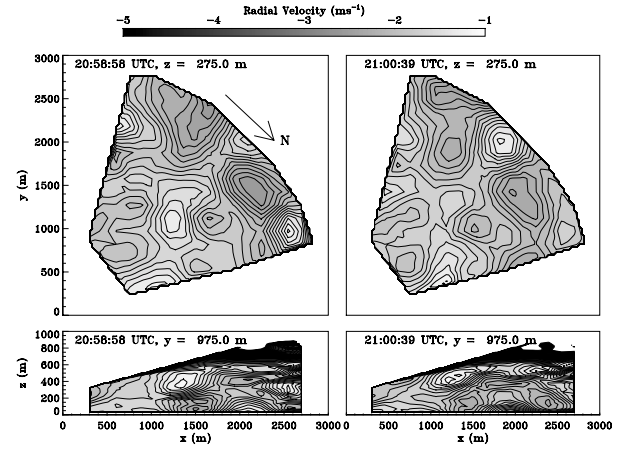


Figure 1 Sample cross sections of $u_r^{obs}(t, \mathbf{r})$ used in the assimilation experiments. The left panels show horizontal (top) and vertical (bottom) cross sections at the start of the assimilation period (20:58:58 UTC). The right panels show horizontal (top) and vertical (bottom) cross sections at the end of the assimilation period (21:00:39 UTC).

Application of the 4DVAR algorithm requires that the radial velocity measurements be interpolated to the forward-model grid. This was accomplished by first removing radial velocity estimates corresponding to low SNR or hard target returns. The remaining data was then spatially and temporally interpolated to the forward model grid using a Cressmen filtering method.

Each volume scan required approximately 90 seconds to complete. An assimilation time window of 100 s was chosen in order to include enough information from two consecutive volume scans. An integration step size of $\Delta t = 2$ s was used to integrate the forward model and the adjoint equations. Thus, 50 time steps were used in the assimilation. The Cressmen filter was applied simultaneously in time and space to interpolate the radial velocity data to each time step and grid point. The horizontal and vertical radii of influence were set equal to twice the horizontal and vertical grid

resolutions, respectively. The temporal “radius of influence” was set equal to 30 s.

The mean state of the boundary layer during the assimilation time is shown in Fig 2. The base state potential temperature $\theta_o(z)$ was obtained from a 1900 UTC sounding at the main site. Profiles of the mean wind speed and direction were computed from the lidar volume scan data using a modified VAD processing technique (Banta et al. 2002). Winds below 600 m AGL were light and westerly. The profile of $\theta_o(z)$ indicates a shallow mixed layer with a strong capping inversion near 600 m AGL. In the stable layer above 600 m AGL the wind speed increased sharply and the wind direction shifted toward southerly at the top of domain.

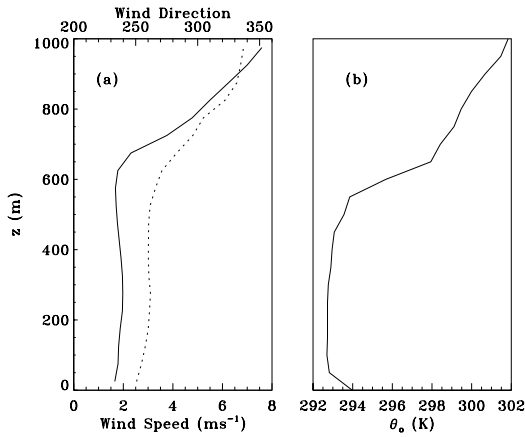


Figure 2 (a) Mean wind speed (solid) and wind direction (dotted) during the assimilation period. (b) the base state potential temperature profile $\theta_o(z)$ from a 1900 UTC sounding at the main CASES-99 site.

5.2 Eddy viscosity

The 4DVAR algorithm used here requires specification of vertical profiles of ν and κ . A more generalized form of the forward model was used to obtain reasonable estimates of these profiles. This more generalized model uses different versions of the Smagorinski turbulence parameterization scheme. In the generalized model equations (2) and (4) were replaced by

$$H_i = \frac{g \delta_{i3}}{\Theta_{ref}} (\theta - \langle \theta \rangle) + \frac{\partial}{\partial x_j} (2\nu S_{ij} - u_i u_j) \quad (12)$$

$$\frac{\partial \theta}{\partial t} = \frac{\partial}{\partial x_j} \left(\kappa \frac{\partial \theta}{\partial x_j} - u_j \theta \right) \quad (13)$$

respectively. In (12) $\langle \theta \rangle$ is the horizontally averaged potential temperature, which depends on both z and t .

The generalized model assumes the same boundary conditions used by the forward model. Runs were performed with homogeneous initialization using the mean wind and temperature profiles shown in Fig 2. Random temperature perturbations on the order of 0.5K were added to the initial temperature field in order to initiate eddy motions. Approximately one half hour of

simulation time was used to spin-up the dynamics. At the end of that time, horizontally averaged profiles of ν and κ were computed. These profiles were then used in the assimilation trials with real lidar data.

We examine the sensitivity of the retrieved velocity and temperature fields to changes in the prescribed eddy viscosity profile by using different versions of the basic Smagorinski SGS scheme in the more general model. The first version we consider is a scheme adopted in RAMS. This scheme uses a stability correction based on the Richardson number, Ri ,

$$\nu = (c\Delta)^2 \sqrt{2S_{ij}S_{ij}} \max(0, 1 - \alpha Ri). \quad (14)$$

In (14) $\Delta = (\Delta x \Delta y \Delta z)^{1/3}$ and α is a specified ratio of eddy diffusivity to eddy diffusion. In the simulations performed here we set $\alpha = 3$ and $c = 0.18$.

The second variation we consider does not involve a stability correction factor but instead removes the effect of the horizontal mean strain rate, $\langle S_{ij} \rangle$ as suggested by Deardorf (1971). This is given by

$$\nu = (c\Delta)^2 \sqrt{2(S_{ij} - \langle S_{ij} \rangle)(S_{ij} - \langle S_{ij} \rangle)}. \quad (15)$$

Equation (15) results in zero production of SGS energy if the resolved turbulence disappears.

Figure 3 shows vertical profiles of horizontally averaged ν from (14) (curve i) and (15) (curve iii). We also show a constant eddy viscosity profile computed by averaging (14) horizontally and vertically (curve ii).

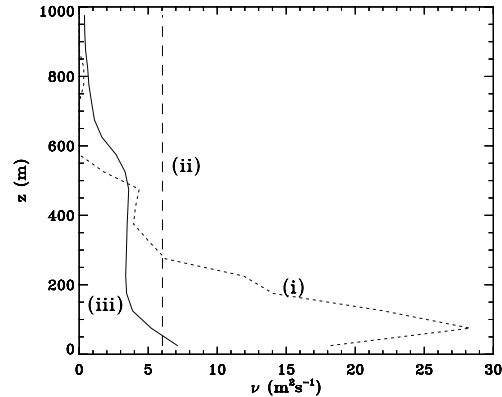


Figure 3 Eddy viscosity profiles used in the assimilation trials. (i) was obtained by horizontally averaging equation (14). (iii) was obtained by horizontally averaging equation (15). (ii) is the vertical average of curve (i).

5.3 Results

Figure 4 shows horizontal and vertical cross sections of the retrieved perturbation velocity fields during the middle of the assimilation period. The first guess for the initial velocity field was provided by the mean winds shown in Fig 2a (corrected for the rotation of the model coordinate system). Generally, the 4DVAR retrieval algorithm converged to an optimal set of initial conditions after approximately 20 to 30 iterations of the minimization algorithm (corresponding to 20 to 30

integrations of the adjoint equations). The cost function descended about two orders of magnitude from its initial "first guess" value.

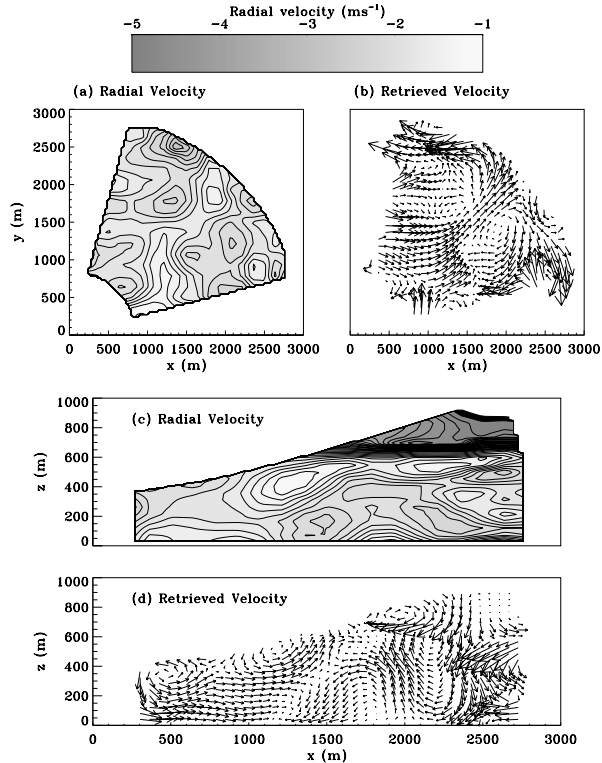


Figure 4 Comparison between the observed radial velocity and retrieved perturbation velocity from the middle of the assimilation period (20:58:48 UTC) using curve (i) in Fig 3 for v . (a) and (b) are horizontal cross sections at $z=300\text{m}$ AGL. (c) and (d) are vertical cross sections at $y=1000\text{ m}$.

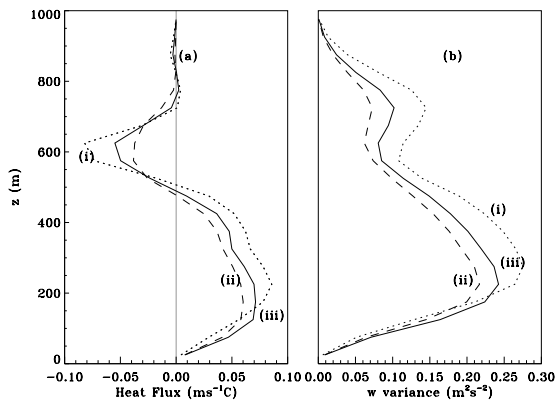


Figure 5 Resolved scale kinematic heat flux (a) and vertical velocity variance (b) for assimilation trials using curves (i), (ii) and (iii) three different assimilation runs.

Comparisons between the measured radial velocity and retrieved velocity fields are shown in Fig 4. The vertical structure of the observed radial velocity field (Fig 4c) shows slightly elevated values at the inversion base.

In Fig 4d the retrieved velocity field indicates strong horizontal divergence in this layer.

Retrievals performed using the three curves in Fig 3 for v did not give dramatically different results. Qualitatively, this agrees with results obtained by Lin et al. (2001) using simulated data. Subtle differences between the retrievals are more evident in horizontally averaged statistics. Figure 5a shows a comparison between the resolved-scale kinematic heat fluxes for the retrieval using the three eddy viscosity profiles shown in Fig 3. A similar comparison is shown for the vertical velocity variance (Fig 5b). The retrieval using an eddy viscosity profile based on equation (14) (curve i) exhibits the most extreme values in both w variance and heat flux. The retrieval using a constant eddy viscosity profile (curve ii) exhibits the smallest variations in both w variance and heat flux.

6. SUMMARY

This paper has described a 4DVAR algorithm used for retrieval of wind and temperature fields from single-Doppler lidar data. The algorithm incorporates a variable eddy viscosity into the Reynolds stress. As a simplifying assumption the eddy diffusion ν and diffusivity κ coefficients are prescribed and dependent only on height. Three assimilation trials were conducted using three different profiles of ν and κ . The retrieved wind and temperature fields exhibit only small differences between the three trials. The resolved scale heat fluxes and vertical velocity variances exhibit similar vertical structure between the three trials but differ in magnitude.

Acknowledgements. This work was supported by the National Science Foundation under grant # ATM-9908453). Funding for field measurements was provided by the Army Research Office, and the Center for Geosciences/Atmospheric Research at Colorado State University. The authors are indebted to Dr. Juanzhen Sun of NCAR.

REFERENCES

- Banta, R.M., R.K. Newsom, J.K. Lundquist, Y.L. Pichugina, R.L. Coulter, and L.D. Mahrt, 2002: Nocturnal low-level jet characteristics over Kansas during CASES-99. *Boundary-Layer Meteor.*, in press.
- Deardorf J.W. 1971: Numerical Investigation of Neutral and Unstable Planetary Boundary Layers. *J. Atmos. Sci.*, **29**, 91-115.
- Harlow F. H. and J. E. Welch, 1965: Numerical Calculation of Time-Dependent Viscous Incompressible Flow of Fluid with Free Surface. *Phys. Fluids*, **8**, 2182-2189.
- Lin C.L., T. Chai, J. Sun 2001: Retrieval of Flow Structure in a Convective Boundary Layer Using and Adjoint Model: Identical Twin Experiments. *J. Atmos. Sci.*, **58**, 1767-1783.
- Sun J., D. W. Flicker, D. K. Lilly, 1991: Recovery of three-dimensional wind and temperature fields from simulated single-Doppler radar data. *J. Atmos. Sci.*, **48**, 876-890.
- , A. Crook, 1994: Wind and thermodynamic retrieval from single-Doppler measurements of a gust front observed during Phoenix II. *Mon. Wea. Rev.*, **122**, 1075-1091.

